

# Dark solitons near the Mott-insulator–superfluid phase transition

Konstantin V. Krutitsky<sup>1</sup>, Jonas Larson<sup>2</sup>, and Maciej Lewenstein<sup>3,4</sup>

<sup>1</sup>*Fachbereich Physik der Universität Duisburg-Essen,*

*Campus Duisburg, Lotharstraße 1, 47048 Duisburg, Germany*

<sup>2</sup>*NORDITA, 106 91 Stockholm, Sweden*

<sup>3</sup>*ICFO-Institut de Ciències de Fotòniques, 008860 Castelldefels (Barcelona), Spain and*

<sup>4</sup>*ICREA-Institució Catalana de Recerca i Estudis Avançats, Lluís Companys 23, 08010 Barcelona, Spain*

(Dated: July 3, 2009)

Dark solitons of ultracold bosons in the vicinity of the Mott-insulator–superfluid phase transition are studied. Making use of the Gutzwiller ansatz we have found antisymmetric eigenstates corresponding to standing solitons, as well as propagating solitons created by phase imprinting. The properties of both types of solitons are studied and in particular it is demonstrated that quantum fluctuations greatly affect the characteristics of the solitons.

PACS numbers: 03.75.-b, 03.75.Lm, 05.45.Yv

*Introduction.*– Ultracold atomic gases provide a perfect playground to study nonlinear atom optics, and nonlinear structures and textures, such as solitons [1, 2]. These studies have led to the observations of dark [3, 4] and bright [5] solitons in trapped Bose-Einstein condensates, or more recently, bright solitons stabilized by the presence of dark ones [6]. The analogy to nonlinear optics [2] has triggered theoretical interest in discrete (lattice) solitons [7, 8], and has led to the seminal observations of gap solitons, i.e., lattice solitons with repulsive interactions, but with an appropriate dispersion management [9].

While most of the studies of solitons were concentrated on their classical aspects, more recently, considerable interest has been devoted to the role of thermal noise [8, 10], quantum properties of solitons and the role of quantum fluctuations. The latter may cause filling up of the dark soliton core in the quantum detection process, as was shown using the Bogoliubov-de Gennes (BdG) equations [11]. The BdG method was also employed to study the stability of solitons [12], excitations caused by the trap opening [13], and entanglement generation in collisions of two bright solitons [14]. A noisy version of the standing bright solitons was studied using the exact diagonalization and quantum Monte Carlo method [15]. Bright soliton in 1D were considered in Ref. [13], where exact Lieb-Liniger solutions were used to calculate the internal correlation function of the particles positions. Making use of the discrete nonlinear Schrödinger equation (DNSE), and the time-evolving block decimation algorithm [16] it was demonstrated that quantum effects lead the soliton to fill in, and that soliton collisions become inelastic [17].

All the previous studies of lattice solitons were done deep in the superfluid phase. However, near the phase boundary between superfluid (SF) and Mott insulator (MI) [18], the propagation of matter waves becomes strongly suppressed due to the enhancement of quantum fluctuations. In general, the properties of solitons in this regime are expected to be very different from the ones far in the SF regime. The aim of the present work is to study lattice solitons near the MI-SF phase tran-

sition. This is done employing the position-dependent Gutzwiller ansatz which gives a satisfactory description of the quantum phases of inhomogeneous bosonic systems [19, 20] as well as their dynamical behavior [21]. The method was recently utilized to study vortices in the vicinity of the MI-SF phase transition [22].

*The model.*– We consider a system of ultracold interacting bosons in a  $d$ -dimensional lattice described by the Bose-Hubbard Hamiltonian

$$\hat{H} = -J \sum_{\langle \mathbf{i}, \mathbf{j} \rangle} \hat{a}_{\mathbf{i}}^{\dagger} \hat{a}_{\mathbf{j}} + \frac{U}{2} \sum_{\mathbf{i}} \hat{a}_{\mathbf{i}}^{\dagger} \hat{a}_{\mathbf{i}}^{\dagger} \hat{a}_{\mathbf{i}} \hat{a}_{\mathbf{i}} - \mu \sum_{\mathbf{i}} \hat{a}_{\mathbf{i}}^{\dagger} \hat{a}_{\mathbf{i}}, \quad (1)$$

where  $J$  is the tunneling matrix element,  $U$  is the on-site atom-atom interaction energy, and  $\mu$  the chemical potential. Throughout the paper, we will be dealing with repulsive interaction, i.e.,  $U > 0$ . The annihilation and creation operators at site  $\mathbf{i}$ ,  $\hat{a}_{\mathbf{i}}$  and  $\hat{a}_{\mathbf{i}}^{\dagger}$ , obey the bosonic commutation relations.

Our analysis employs the Gutzwiller ansatz. Thereby, eigenstates of the Hamiltonian (1) are taken as products of local states  $|\Phi\rangle = \prod_{\mathbf{i}} |s_{\mathbf{i}}\rangle$ ,  $|s_{\mathbf{i}}\rangle = \sum_{n=0}^{\infty} c_{in} |n\rangle_{\mathbf{i}}$ . Here,  $|n\rangle_{\mathbf{i}}$  is the Fock state with  $n$  atoms at site  $\mathbf{i}$ . We are interested in the solutions which has a position-dependence only in one spatial dimension. Then the equations of motion [19, 20, 23] take the form

$$\begin{aligned} i\hbar \frac{dc_{in}}{dt} = & -J[\psi_{i-1}^* + \psi_{i+1}^* + 2(d-1)\psi_i^*] \sqrt{n+1} c_{i,n+1} \\ & -J[\psi_{i-1} + \psi_{i+1} + 2(d-1)\psi_i] \sqrt{n} c_{i,n-1} \\ & + \left[ \frac{U}{2} n(n-1) - \mu n \right] c_{in}, \end{aligned} \quad (2)$$

where  $\psi_i = \sum_{n=1}^{\infty} c_{i,n-1}^* c_{in} \sqrt{n}$  is the condensate order parameter.

*Standing solitons.*– Stationary solutions of Eqs. (2) are worked out for a lattice with the finite number of sites  $L$  and with the boundary conditions  $c_{0,n} = c_{1,n}$ ,  $c_{L+1,n} = c_{L,n}$ , for any  $n$ . In the ground state, the coefficients  $c_{in}$  and the order parameter  $\psi_i$  do not depend on the site index  $i$ . The boundaries between the MI and

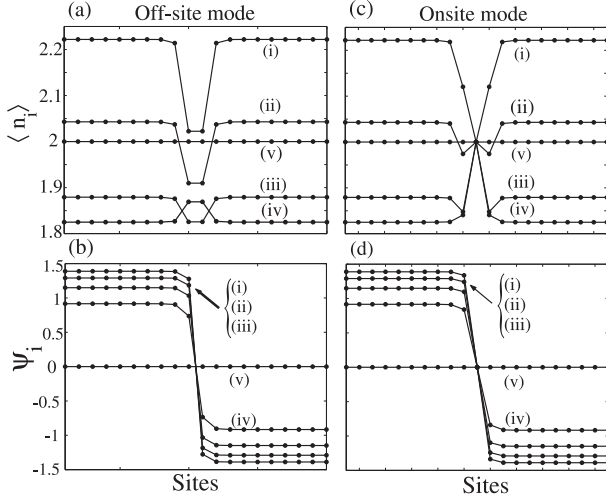


FIG. 1: Mean number of atoms  $\langle \hat{n}_i \rangle$  (a) and (c), and mean-field order parameter  $\psi_i$  (b) and (d). The scaled chemical potential  $\mu/U = 1.2$  and the tunneling rates  $2dJ/U$ : 0.7 (i), 0.5 (ii), 0.3 (iii), 0.15 (iv), and 0.05 (v).

SF are determined by  $2dJ_c/U = (n_0 - \mu/U)(\mu/U - n_0 + 1)/(1 + \mu/U)$ , where  $n_0$  is the smallest integer greater than  $\mu/U$ . For  $J < J_c$ , the ground state is MI, where  $c_{in} = \delta_{n,n_0} \exp(-i\omega_n t)$ ,  $\hbar\omega_n = Un(n-1)/2 - \mu n$ ,  $\psi_i = 0$ .

In the present work, we are interested in the low-energy excited eigenstates, where the order parameters  $\psi_i$  are anti-symmetric with respect to the middle point of the lattice. These are the kink states which can be treated as standing dark solitons. In the Gutzwiller ansatz, the excited states of the MI are products of local Fock states, where the occupation numbers  $n_i$  can be different from  $n_0$ . As a consequence, all  $\psi_i$  vanish again and the soliton solutions are lacking for the values of the parameters within this regime.

In the SF, the situation is different and one has to distinguish between two cases: when the middle point is on the lattice site (onsite modes) and in the middle of two neighboring sites (off-site modes). The two modes have different energies, and the difference defines the Peierls-Nabarro barrier [24]. In the present work, we will be dealing only with situations where the presence of the barrier is not relevant.

Typical examples of standing onsite as well as off-site soliton modes are displayed in Fig. 1. The mean occupation numbers  $\langle \hat{n}_i \rangle$  are shown in (a) and (c), while (b) and (d) give the associated mean-field order parameters  $\psi_i$ . The individual curves correspond to different tunneling rates  $J$ . For the considered chemical potential,  $\mu/U = 1.2$ , the MI-SF transition occurs at  $2dJ/U \approx 0.0727$ . Above this value, in the SF regime, solitons are indeed found as depicted in Fig. 1(b) and (d). In the numerical calculations,  $n$  in Eq. (2) is restricted by some finite  $N$  ( $c_{i,N+1} = 0$ ). The computations are performed using the imaginary time propagation technique.

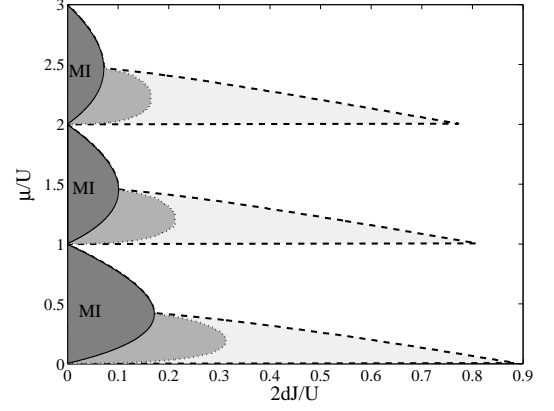


FIG. 2: Dark areas bounded by the solid lines show the first three MI zones. Gray areas between solid and dotted lines indicate the regions where the off-site solitons have a local maximum of the mean occupation number at the middle lattice sites. The light gray areas between solid and dashed lines depict the same for on-site solitons. In the rest part of the diagram the mean particle number takes the minimal value at the middle site(s).

The size of the lattice  $L$  as well as the cut-off number of atoms  $N$  at each site where chosen large enough such that their influences on the eigenstates are negligible. The dimension is  $d = 3$  for these examples and throughout the paper.

In the present work, we consider the parameters range near the MI-SF transition where quantum fluctuations are especially important. An outcome of this is that the mean occupation numbers  $\langle \hat{n}_i \rangle$  are not equal to the mean number of condensed atoms  $|\psi_i|^2$  as it would in the mean-field description valid deep in the SF phase. The relation between  $\psi_i$  and the expansion coefficients  $c_{i,n}$  is given after Eq. (2). For example, the non-zero occupation number, despite  $\psi_i = 0$ , is clearly seen from Fig. 1 (a) and (b). For the onsite mode, when  $\psi_i$  vanishes at the middle site, the state of the corresponding site is a Fock state. In the example of Fig. 1, this is the Fock state with  $n = 2$ . On the other hand, for the off-site mode we have  $\psi_i \neq 0$  for all  $i$ 's in the SF regime and thereby the onsite states are never pure Fock states. Far in the SF regime, the occupation numbers attain a global minimum at the middle lattice site(s). Surprisingly, by approaching the MI boundaries the global minimum turns into two local minima at the neighboring sites. Even closer to the critical point, a global maximum is formed at the middle lattice site(s). We distinguish these localized modes from the ones with a single global minimum at the middle site(s). Fig. 2 depicts a  $(\mu, J)$  diagram identifying the various types of solutions. The anomalous regions where the mean occupation numbers have local maxima are located near the lower branches of the MI-lobes corresponding to the hole excitations [25] which support dark solitons.

*Propagating solitons created by phase imprinting.* – Ex-

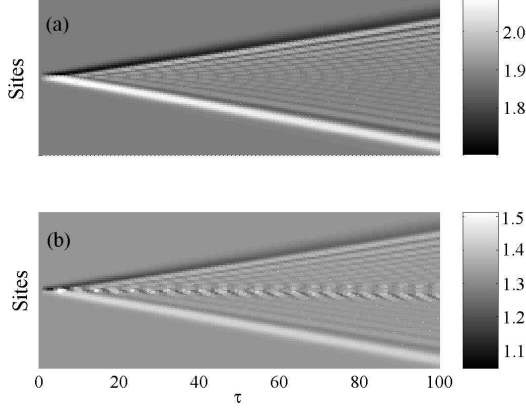


FIG. 3: Time evolution of the mean occupation numbers  $\langle \hat{n}_i \rangle$  (a) and the order parameters  $|\psi_i|^2$  (b) after phase imprinting with  $\Delta\phi = \pi$ ,  $l_{imp} = 2$ . The parameters are  $\mu/U = 1.2$ ,  $2dJ/U = 0.3$ , giving similar evolution for both  $\langle \hat{n}_i \rangle$  and  $|\psi_i|^2$ . The spatial region (vertical axis) contains 80 lattice sites, and the dimensionless time  $\tau = tU/\hbar$ .

perimentally, dark (or gray) solitons are typically created via a phase-imprinting method [3]. Initially ( $t = 0$ ) the system of atoms is assumed to be in its ground state. During a short time  $t_{imp}$  one applies a spatially dependent potential on top of the lattice. In the Bose-Hubbard Hamiltonian, it is described by the term  $\sum_i \epsilon_i a_i^\dagger a_i$ . If the time  $t_{imp}$  is much shorter than other characteristic time scales, from Eqs. (2) we get that it induces a shift in the phase of the atomic states

$$\begin{aligned} c_{ln}(t_{imp}) &= c_{ln}(0) \exp\left(-i \frac{\epsilon_l t_{imp}}{\hbar} n\right), \\ \psi_l(t_{imp}) &= \psi_l(0) \exp\left(-i \frac{\epsilon_l t_{imp}}{\hbar}\right). \end{aligned} \quad (3)$$

For the creation of dark solitons we choose a hyperbolic tangent imprinting potential, such that

$$\phi_l = \frac{\epsilon_l t_{imp}}{\hbar} = \frac{\Delta\phi}{2} \left[ 1 + \tanh\left(\frac{l}{0.45l_{imp}}\right) \right]. \quad (4)$$

Here,  $l_{imp}$  is the width of the interval around  $l = 0$ , where  $\phi_l/\Delta\phi$  grows from 0.1 to 0.9 [26]. Apart from the moving gray soliton, the phase imprinting also induces a density wave propagating in the opposite direction to the soliton [3, 26].

Figs. 3, 4, 5 present the time evolution of the occupation numbers  $\langle \hat{n}_i \rangle$  and squared absolute values of the mean-field order parameters  $|\psi_i|^2$  for two different values of  $J$  and  $\mu$ . Scaling  $\mu$  and  $J$  by  $U$ , we work with a dimensionless time  $\tau = tU/\hbar$ . In Fig. 3,  $J$  is taken relatively large but still in the regime where the on-site modes have local maxima of  $\langle \hat{n}_i \rangle$  (light gray region in Fig. 2). In this case, the outcomes of quantum fluctuations are small and the dips and the maxima of  $\langle \hat{n}_i \rangle$  coincide with those of

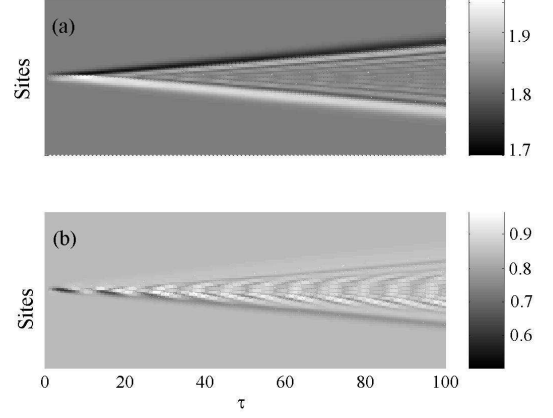


FIG. 4: Same as in Fig. 3, but with  $2dJ/U = 0.15$ . In this regime, the directions of propagating maximum and minimum of  $|\psi_i|^2$  and  $\langle \hat{n}_i \rangle$  seen in Fig. 3 are reversed.  $\tau$  is the scaled dimensionless time.

$|\psi_i|^2$ . We note that the dips propagate slower than the maxima. This type of dynamics is always recovered in simulations based on the DNSE.

In Fig. 4, the value of  $\mu$  is the same as in Fig. 3 but  $J$  is smaller such that we enter into the gray region of Fig. 2. The overall structure of  $\langle \hat{n}_i \rangle$  remains the same as in the example shown in Fig. 3, but here  $|\psi_i|^2$  behaves differently. More precisely,  $|\psi_i|^2$  shows a local maximum coinciding with the propagating dip of the occupation numbers, and a local minimum where instead  $\langle \hat{n}_i \rangle$  has a local maximum. Furthermore, the dip of  $\langle \hat{n}_i \rangle$  propagates faster than its maximum moving in the opposite direction. This anomalous behavior, which is found only within the gray regions of Fig. 2, cannot be described by the DNSE. Closer to the boundary of the gray region as in the example depicted in Fig. 5,  $|\psi_i|^2$  can become oscillating and spreading around the imprinting site, while  $\langle \hat{n}_i \rangle$  still shows similar dynamics as in Figs. 3 and 4. In the remaining white regions of Fig. 2, the time evolution is qualitatively the same as in Fig. 3.

We also performed simulations with other values of  $l_{imp}$  and did not find any strong influence on the propagation velocity. Larger values of  $l_{imp}$  result in broader propagating modes and their shapes become more smooth. The interference pattern between the modes propagating in the opposite directions, visible in the center of Figs. 3, 4, 5, becomes suppressed for larger  $l_{imp}$ .

Finally, the soliton velocity  $v_{sol}$  as well as the velocity of the density wave  $v_{dens}$  as functions of  $\Delta\phi$  are shown in Fig. 6. They are calculated making use of a linear fit of the corresponding minimum and maximum of  $\langle \hat{n}_i \rangle$  for the dimensionless time  $\tau = tU/\hbar > 10$ . Although the dependences are very weak, it is found that the velocities are not monotonic showing a maximum for  $\Delta\phi \approx \pi/4$ . This behaviour is different from what was found in the simulations based on the Gross-Pitaevskii equation in continuum in a harmonic trap [3] or in a periodic potential [12].

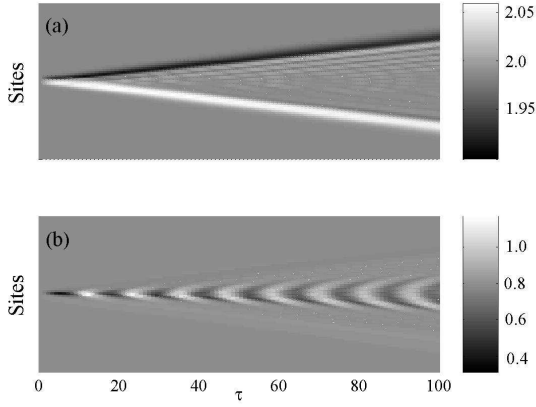


FIG. 5: Same as in Figs. 3 and 4, but with  $\mu/U = 1.4$ ,  $2dJ/U = 0.15$ . For these parameters,  $|\psi_i|^2$  oscillates and spreads near the imprinting site. Time  $\tau$  is dimensionless.

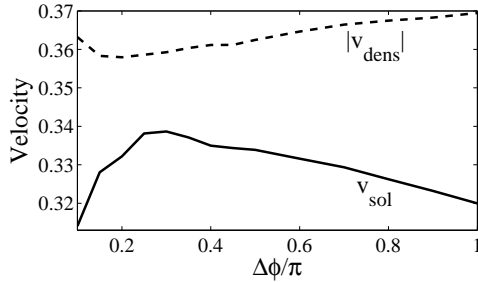


FIG. 6: Dimensionless velocity of the soliton (solid line) and density (dashed line) modes as a function of  $\Delta\phi$ . Here  $2dJ/U = 0.3$ ,  $\mu/U = 1.2$ , and  $l_{imp} = 2$ .

With the decrease of  $\Delta\phi$  the propagation velocity slightly increases (Fig. 6). On the other hand, the depth of the propagating dip as well as the height of the maxima decreases. The same was found in continuum model [3].

*Conclusion.*— We have investigated dark solitons of bosons in optical lattices at zero temperature. Using the Gutzwiller ansatz, we found kink stationary states where the condensate order parameter  $\psi_i$  is antisymmetric function with respect to some spatial point. However, in certain regions close to the MI-SF transition which are shown in Fig. 2, the corresponding  $n_i$  does not have a global minimum at the point where  $\psi_i$  vanishes. This anomalous behavior shows up near the phase boundary where quantum fluctuations play an important role.

The real-time dynamics of the propagating dark solitons created by the phase imprinting is studied as well. In the MI phase, the solitons cannot be created. This can be done only in the SF phase, where there are always global minima and maxima of  $n_i$  propagating in the opposite directions and these directions are always the same. The behavior of the condensate can be different and this happens in the anomalous regions of the off-site stationary modes shown as gray areas in Fig. 2.

*Acknowledgments.*— We would like to thank R. Graham and B. Malomed for helpful discussions. The work of KK was supported by the SFB/TR 12 of the German Research Foundation (DFG). JL acknowledges support from VR-Vetenskapsrådet and the MEC program (FIS2005-04627). ML acknowledges Spanish MEC/MINCIN projects TOQATA (FIS2008-00784) and QOIT (Consolider Ingenio 2010), ESF/MEC project FERMIX (FIS2007-29996-E), EU STREP project NAMEQUAM, ERC Advanced Grant QUAGATUA, and Alexander von Humboldt Foundation Senior Research Prize.

- 
- [1] L. P. Pitaevskii and S. Stringari, *Bose-Einstein Condensation*, Oxford University Press, Oxford, 2003.
  - [2] Y. S. Kivshar and G. P. Agrawal, *Optical Solitons: From Fibers to Photonic Crystals*, Academic Press, 2003.
  - [3] S. Burger *et al.*, Phys. Rev. Lett. **83**, 5198 (1999).
  - [4] J. Denschlag *et al.*, Science **287**, 97 (2000).
  - [5] L. Khaykovich *et al.*, Science **296**, 1290 (2002); K. E. Strecker, *et al.*, Nature **417**, 150 (2002).
  - [6] C. Becker *et al.*, Nature Physics **4**, 496 (2008).
  - [7] A. Trombettoni *et al.*, Phys. Rev. Lett. **86**, 2353 (2001).
  - [8] V. Ahufinger *et al.*, Phys. Rev. Lett. **94**, 130403 (2005).
  - [9] B. Eiermann *et al.*, Phys. Rev. Lett. **92**, 230401 (2004).
  - [10] A. Muryshv *et al.*, Phys. Rev. Lett. **89**, 110401 (2002).
  - [11] J. Dziarmaga, Phys. Rev. A **70**, 063616 (2004).
  - [12] A. V. Yulin *et al.*, Phys. Rev. A **67**, 023611 (2003).
  - [13] Y. Castin, Eur. Phys. J. B **68**, 317 (2009).
  - [14] M. Lewenstein and B. A. Malomed, arXiv:0901.2836.
  - [15] J. Javanainen *et al.*, Phys. Rev. Lett. **101**, 170405 (2008).
  - [16] G. Vidal, Phys. Rev. Lett. **93**, 040502 (2004).
  - [17] R. V. Mishmash *et al.*, arXiv:0710.0045; *ibid.* arXiv:0810.2593; *ibid.* arXiv:0906.4949.
  - [18] M. P. A. Fisher *et al.*, Phys. Rev. B **40**, 546 (1989).
  - [19] D. Jaksch *et al.*, Phys. Rev. Lett. **81**, 3108 (1998).
  - [20] P. Buonsante *et al.*, Phys. Rev. A **76**, 011602(R) (2007).
  - [21] J. Zakrzewski, Phys. Rev. A **71**, 043601 (2005).
  - [22] D. S. Goldbaum *et al.*, Phys. Rev. A **79**, 021602(R) (2009); E. Lundh, Eur. Phys. Lett. in press (2009).
  - [23] B. Damski *et al.*, Phys. Rev. Lett. **91**, 080403 (2003).
  - [24] Y. S. Kivshar *et al.*, Phys. Rev. E **50**, 5020 (1994).
  - [25] J. K. Freericks and H. Monien, Europhys. Lett. **26**, 545 (1994); Phys. Rev. B **53**, 2691 (1996).
  - [26] S. Burger *et al.*, Phys. Rev. A **65**, 043611 (2002).